Magnetic Damping Properties of Single-Crystalline $Co_{55}Mn_{18}Ga_{27}$ and $Co_{50}Mn_{18}Ga_{32}$ Films

Jia-Rui Chen(陈家瑞)[1], Yu-Ting Gong(龚钰婷)[2], Xian-Yang Lu(陆显扬)[2*], Chen-Yu Zhang(张晨宇)[3], Yong Hu(胡勇)[3*], Ming-Zhi Wang(王铭志)[4], Zhong Shi(时钟)[4], Shuai Fu(付帅)[1], Hong-Ling Cai(蔡宏灵)[1,5], Ruo-Bai Liu(刘若柏)[1], Yuan Yuan(袁源)[1], Yu Lu(卢羽)[1], Tian-Yu Liu(刘天宇)[1], Biao You(游彪)[1,5], Yong-Bing Xu(徐永兵), and Jun Du(杜军)[1,5*]

[1]*National Laboratory of Solid State Microstructures and Department of Physics, Nanjing University, Nanjing 210093, China*
[2]*York-Nanjing Joint Center (YNJC) for Spintronics and Nano-Engineering, School of Electronic Science and Engineering, Nanjing University, Nanjing 210093, China*
[3]*College of Sciences, Northeastern University, Shenyang 110819, China*
[4]*School of Physics Science and Engineering, Tongji University, Shanghai 200092, China*
[5]*Collaborative Innovation Center of Advanced Microstructures, Nanjing 210093, China*

(Received 26 January 2023; accepted manuscript online 8 March 2023)

We investigate the structural, static magnetic and damping properties in two Mn-deficient magnetic Weyl semimetal Co-Mn-Ga (CMG) alloy films, i.e., $Co_{55}Mn_{18}Ga_{27}$ (CMG1) and $Co_{50}Mn_{18}Ga_{32}$ (CMG2), which were epitaxially grown on MgO (001) substrates. CMG1 has a mixing phase of $B2$ and $L2_1$, larger saturation magnetization ($M_s \sim 760\,\mathrm{emu/cm^3}$), stronger in-plane magnetic anisotropy. CMG2 has an almost pure $B2$ phase, smaller M_s ($\sim 330\,\mathrm{emu/cm^3}$), negligible in-plane magnetic anisotropy. Time-resolved magneto-optical Kerr effect results unambiguously demonstrate an obvious perpendicular standing spin wave (PSSW) mode in addition to the Kittel mode for both of the CMG films. The intrinsic damping constant is about 0.0055 and 0.015 for CMG1 and CMG2, respectively, which are both significantly larger than that of the stoichiometric CMG (i.e., Co_2MnGa) film reported previously. In combination with the first-principles calculations, the intrinsic damping properties of the Mn-deficient CMG films can be well explained by considering the increase of density of states at the Fermi level, reduction of M_s, and excitation of the PSSW mode. These findings provide a new clue to tuning the magnetic damping of the magnetic Weyl semimetal film through slight off-stoichiometry.

DOI: 10.1088/0256-307X/40/4/047501

Very recently, Heusler alloy Co_2MnGa film has received significant attention[1–12] due to the following several reasons. Firstly, it is a magnetic Weyl semimetal with large Berry curvature distribution around the Fermi energy,[4–6] hence some intriguing transport phenomena, such as the giant intrinsic anomalous Hall effect,[7,8] the anomalous Nernst effect,[7,9] magneto-optical responses,[10] and the chiral anomaly,[11,12] have been observed. Secondly, large spin polarization and low magnetic damping could be obtained in the Co_2MnGa film due to its very small density of states (DOS) of spin minority subband at the Fermi level.[13–15] Last but not least, bulk Co_2MnGa has a high Curie temperature $T_c \sim 694$ K[7] and a relatively large saturation magnetization ($M_s \sim 780\,\mathrm{emu/cm^3}$).[16] These properties make the Co_2MnGa film a good candidate for promising spintronic applications in spin-orbit-torque (SOT), spin-transfer-torque (STT), and magnonics-based devices.[17–19]

Magnetic damping constant α plays a significant role in magnetic precession and spin relaxation process.[20–25] On the one hand, α is a key factor determining the magnetization reversal speed, and increasing α can substantially reduce the switching time of magnetization.[22,23] On the other hand, decreasing α can lower the critical current density j_{cric} for STT switching because j_{cric} is proportional to α.[24,25] Therefore, tuning α to be an appropriate value is of great importance for developing high performance spintronic devices. To our knowledge, despite the attractive transport properties of Co_2MnGa resulted from its nontrivial topology of the band structure, the experimental exploration of magnetic damping in Co_2MnGa film remains limited. Note that Co_2MnGa has $L2_1$, $B2$ and $A2$ three different phases with the chemical ordering decreased sequentially.[16,19,26,27] Guillemard *et al.* compared the magnetic damping in a series of single-crystalline Co_2MnZ ($Z =$ Si, Ge, Sn, Al, Ga, and Sb) Heusler alloy films and found that α is about 2×10^{-3} in the $L2_1$-ordered Co_2MnGa film, which is the largest among the Co_2MnZ films.[28] Soon after, they reported that α was increased to be 4.5×10^{-3} in the 40-nm-thick poly-crystalline Co_2MnGa film with a mixing phase of $B2$ and $L2_1$.[29] Very recently, Swekis *et al.* investigated the thickness dependence of α in the $L2_1$-ordered Co_2MnGa single-crystalline films and found that α increases slightly with increasing

*Corresponding authors. Email: xylu@nju.edu.cn; huyong@mail.neu.edu.cn; jdu@nju.edu.cn
© 2023 Chinese Physical Society and IOP Publishing Ltd

the thickness and is about 1.4×10^{-3} when the thickness is 40 nm.[30]

Therefrom, it can be seen that the damping constant of Co_2MnGa film is correlated to its chemical ordering, crystallinity and thickness. Furthermore, the stoichiometry may be another important factor influencing the magnetic damping because the band structure of Co_2MnGa will be altered in the case of off-stoichiometry.[31] The theoretical calculations show that the Mn atoms provide a majority of the magnetic moments in the Co_2Mn-based alloys, such as Co_2MnAl, Co_2MnGa, and Co_2MnGe.[32] Therefore, the concentration of Mn in the Co_2MnGa film may substantially affect the M_s value and the damping constant consequently. On the other hand, in previous studies, the α values of Co_2MnGa films were all obtained from the ferromagnetic resonance (FMR) technique by linearly fitting the frequency dependence of linewidth (ΔH). However, two-magnon scattering (TMS) and other extrinsic factors may also be included in the ΔH term, leading to uncertainty in determining the intrinsic α. Alternatively, time-resolved magneto-optical Kerr effect (TRMOKE) is another powerful technique with which the intrinsic α can be achieved under a large external field by greatly suppressing the TMS and other extrinsic contributions.

In this work, two 50-nm-thick Mn-deficient Co-Mn-Ga (CMG) films, i.e., $Co_{55}Mn_{18}Ga_{27}$ (CMG1) and $Co_{50}Mn_{18}Ga_{32}$ (CMG2), were epitaxially grown on MgO (001) single-crystal substrates by magnetron sputtering. The former and the latter can be roughly considered as substituting a small portion of Mn atoms with Co and Ga atoms, respectively. CMG1 has a mixing phase of B_2 and $L2_1$, larger M_s, and stronger in-plane magnetic anisotropy, while CMG2 has an almost pure B_2 phase, smaller M_s, and negligible in-plane magnetic anisotropy. TRMOKE was employed to investigate the damping properties of the two CMG samples. Note that the perpendicular standing spin wave (PSSW) mode could be clearly observed in both of them. Moreover, they both have large intrinsic damping constants, i.e., 5.5×10^{-3} for CMG1 and 0.015 for CMG2. First-principles calculations were performed and the results are in good agreement with the experimental findings.

The $Co_{55}Mn_{18}Ga_{27}$ (CMG1) and $Co_{50}Mn_{18}Ga_{32}$ (CMG2) films with the nominal thickness of 50 nm were deposited on MgO (001) single-crystalline substrates at 700 ℃ by magnetron co-sputtering from a Co target and a $Co_{37}Mn_{34}Ga_{29}$ target. Finally, a 2-nm-thick Al layer was deposited as the capping layer to prevent the CMG films from oxidation. The base pressure was less than 1×10^{-5} Pa and the Ar pressure was kept at 0.3 Pa during the film deposition. The atomic ratios of Co, Mn, and Ga were determined by x-ray fluorescence (XRF) whose sensitivity is about 1%. In comparison with stoichiometric CMG, the Mn concentrations of both CMG1 and CMG2 films are fixed at 18%, and the Mn-deficient sites can be thought of as occupying by Co and Ga atoms, respectively. The structure and chemical ordering of the thin films were characterized by x-ray diffraction (XRD, Bruker D8-Advance). The in-plane magnetic hysteresis (M–H) loops were measured by a superconducting quantum interference device-vibrating sample magnetometer (SQUID-VSM, Quantum Design) and the out-of-plane M–H loops were measured by a VSM (Microsense EV7). The damping properties were characterized by a home-made pump-probe TRMOKE equipment. All the characterizations and measurements were performed at room temperature.

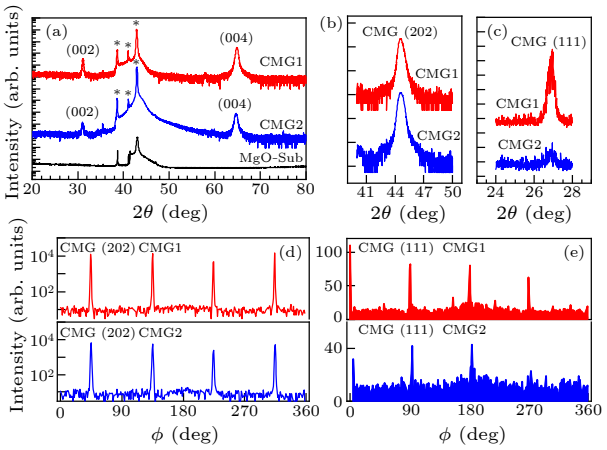

Fig. 1. (a) Out-of-plane XRD patterns of CMG1, CMG2, and MgO (001) substrate. The stars denote the peaks come from the substrate. (b) and (c) XRD patterns of 2θ-scan for CMG(111) and (202) planes by titling (b) $\chi \sim 45°$, $\phi \sim 45°$ and (c) $\chi \sim 54.7°$, $\phi \sim 0°$ for CMG1 and CMG2, respectively. (d) and (e) In-plane (ϕ-scan) XRD patterns of the CMG(202) and the CMG(111) planes for CMG1 and CMG2, respectively.

Figure 1(a) shows the out-of-plane XRD patterns for the CMG films and the MgO (001) substrate. Besides the peaks from the substrate, the 002 and 004 peaks can be clearly observed in both CMG1 and CMG2 films and the peaks from other orientations are all absent, indicating that the CMG films were grown along the (001) orientation on the MgO (001) substrates. Moreover, the strong reflections from the (002) plane also indicate the $B2$-ordering existing in both the CMG films. The lattice constant a is calculated to be 5.74 Å and 5.76 Å for CMG1 and CMG2, respectively, which are both very close to that of bulk Co_2MnGa (5.77 Å).[7,8] By tilting the film surface to $\chi \sim 45°$ and $\chi \sim 54.7°$, XRD patterns for the (202) and (111) planes were detected for the CMG films, as shown in Figs. 1(b) and 1(c), respectively. The (202) peaks are clearly observed in both the samples. However, a strong and a very weak (111) peak are observed in CMG1 and CMG2, respectively, indicating a significant and negligible $L2_1$-ordering in the former and the latter since the presence of superlattice (111) peak is a signature of $L2_1$-ordering.[16] As shown in Figs. 1(d) and 1(e), ϕ-scan measurements have been carried out for the (202) and (111) reflections of the CMG films. The fourfold rotational symmetries of the peaks indicate that the CMG films are grown epitaxially on the MgO (001) substrates. Considering that the lattice constants of CMG and MgO ($a_{MgO} = 4.216$ Å[33]) satisfy $a_{CMG} \approx \sqrt{2}a_{MgO}$, the epitaxial relationship between the CMG films and the MgO sub-

strate is CMG[110]//MgO[100]. From the above results, it can be concluded that CMG1 has a mixing phase of $L2_1$ and $B2$ while CMG2 has an almost pure $B2$ phase, indicating that CMG1 has more chemically ordered structure than CMG2.

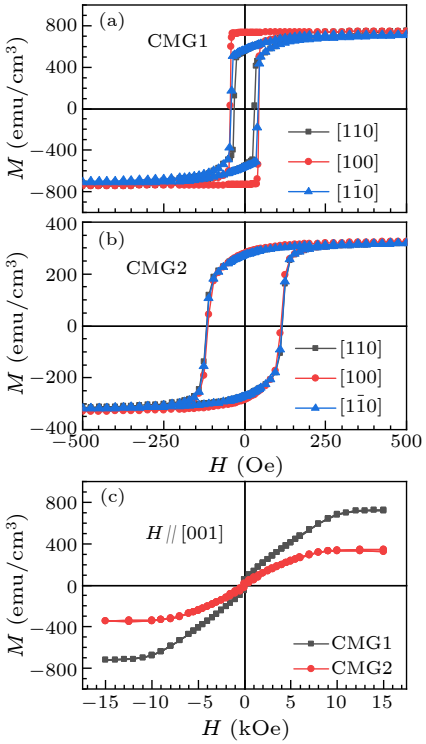

Fig. 2. In-plane M–H loops of CMG1 (a) and CMG2 (b) measured along the crystallographic axes of [110], [100] and [1$\bar{1}$0] of the MgO (001) substrate. (c) Out-of-plane M–H loops of CMG1 and CMG2.

Figures 2(a) and 2(b) show the in-plane M–H loops of the CMG films when the external field is applied along three different crystal orientations of [110], [100], and [1$\bar{1}$0] of the MgO substrate. The M_s of CMG1 is about 730 emu/cm^3, which is close to the values reported in the Co_2MnGa film (690 emu/cm^3)[16] and bulk Co_2MnGa (780 emu/cm^3).[16] In contrast, the M_s of CMG2 is only about 330 emu/cm^3, which is much smaller than that of CMG1. On the other hand, the magnetic anisotropies of the two CMG films are also different. For CMG1, the M–H loops measured along the [110] and [1$\bar{1}$0] directions are almost the same, while they are quite different from that measured along the [100] direction, demonstrating an in-plane biaxial magnetic anisotropy. For CMG2, the M–H loops measured along the three directions are almost overlapped together, indicating a negligible in-plane magnetic anisotropy. The different in-plane magnetic anisotropies can be attributed to different magnetocrystalline anisotropies, possibly resulted from the different chemical orderings of the two CMG films. Figure 2(c) shows the out-of-plane M–H loops of the two CMG films when the external field was applied along the [001] direction of the MgO substrate. It can be seen that the saturation magnetic field is obviously larger than $4\pi M_s$ for either CMG1 or CMG2, indicating a negative constant of perpendicular magnetic anisotropy energy.

In this work, laser-induced magnetic dynamics of the CMG films was investigated by TRMOKE. The geometry of the TRMOKE measurement can be found in our previous works.[34–36] Figures 3(a) and 3(b) exhibit several representative magnetic procession curves obtained under various external fields for CMG1 and CMG2, respectively. For each of the samples, the oscillation amplitude increases and decreases periodically with the delay time, clearly demonstrating a beating frequency effect. Thus, the experimental TRMOKE signal can be analyzed by the following formula:[36]

$$\Delta\theta_K \propto \sum_{i=1}^{2} A_i \exp(-t/\tau_i)\sin(2\pi f_i t + \varphi_i) + B(t), \quad (1)$$

where A_i, f_i, τ_i, and φ_i denote the amplitude, frequency, relaxation time, and initial phase of the i-th mode precession, respectively. $B(t)$ represents the background term due to the slow recovery of the magnetization. By taking into account two precession modes with different frequencies ($f_1 < f_2$), the experimental TRMOKE signals can be well fitted according to Eq. (1), as depicted by the solid lines in Figs. 3(a) and 3(b). Moreover, fast Fourier transformation (FFT) analysis is used to explore the multiple-mode Kerr rotation oscillations and the results show clearly that there are two strong resonance peaks, as displayed in Figs. S1(a) and S1(b) in the Supplementary Material for CMG1 and CMG2, respectively. These two frequencies are close to those obtained by directly fitting the TRMOKE signals in terms of Eq. (1), as shown in Fig. S2 in the Supplementary Material.

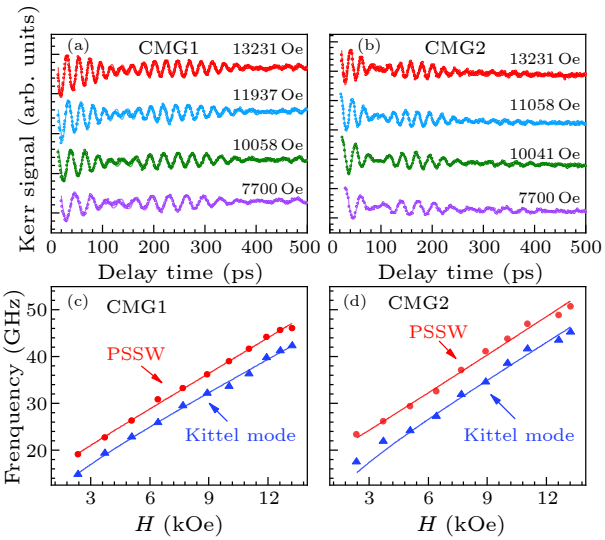

Fig. 3. Measured transient Kerr signal of CMG1 (a) and CMG2 (b) under various external fields. The solid lines show the best fitting using the double damped sinusoidal formula of Eq. (1). Magnetic field dependences of precession frequency for CMG1 (c) and CMG2 (d). The blue (red) dots and lines represent the experimental and fitted results, from the Kittle (PSSW) mode, respectively.

Generally, magnetic precession modes are composed of uniform mode (i.e., Kittel mode) and various types of

spin wave mode, such as PSSW, Damon-Eshbach dipolar surface spin waves (DE modes)[37,38] and TMS. Note that the possibility of DE modes is excluded, as discussed in the Supplementary Material. Moreover, TMS should be greatly suppressed under high external field, otherwise the dual frequency effects clearly occurring under larger external fields (e.g., $H = 13231$ Oe) can hardly be explained. Therefore, the present low-frequency (f_1) and high-frequency (f_2) resonance peaks are considered to result from the Kittel mode and the first-order PSSW mode, respectively. As shown in Figs. 3(c) and 3(d), the frequencies of these two modes obtained from fitting the TRMOKE signals are plotted as a function of the external field strength, which can be well fitted by using the method described in the Supplementary Material of Ref. [36]. Note that the fitting is based on the Landau–Lifshitz–Gilbert equation with taking into account the Zeeman energy, demagnetization energy, perpendicular anisotropy energy and Cubic anisotropy energy. All the fitting parameters, i.e., the perpendicular anisotropy constant K_u, cubic anisotropy constant K_c, g-factor, effective magnetization $4\pi M_{\rm eff}$, and exchange stiffness A are listed in Table 1. These results are comparable to those reported in the Co_2MnGa film.[30] For examples, the g-factor (1.97) and the A value (14.6 pJ/m) are respectively much close to those (1.95, 16.8 pJ/m) for the 80-nm-thick Co_2MnGa film reported in Ref. [30]. In comparison with CMG2, CMG1 has larger K_c, which may be responsible for its in-plane magnetic anisotropy. Moreover, both of the CMG films have considerably negative values of K_u. These fitting parameters are coincident with the M–H loops shown in Fig. 2.

Table 1. Magnetic parameters for CMG1 and CMG2 extracted from fitting the magnetic field dependence of frequency.

Sample	K_u (kJ/m^3)	K_c (kJ/m^3)	g	$4\pi M_{\rm eff}$ (Oe)	A (pJ/m)
CMG1	−148	13.6	1.97	13025	14.7
CMG2	−121	5.65	1.97	12000	14.0

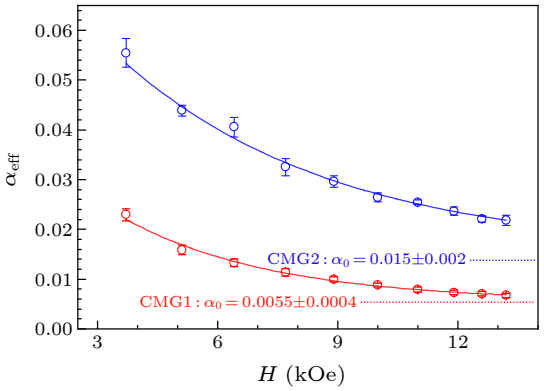

Fig. 4. Characteristics of $\alpha_{\rm eff}$ against the external field for CMG1 (red) and CMG2 (blue). From the single exponential decay fitting (solid lines), the values of intrinsic damping α_0 for both the films are estimated.

The effective damping constants $\alpha_{\rm eff}$ are derived from the Kittel mode using $\alpha_{\rm eff} = 1/2\pi f_1 \tau_1$, where $\alpha_{\rm eff}$, f_1, and τ_1 are the effective damping constant, frequency, and relaxation time of the Kittel mode, respectively. The variations of $\alpha_{\rm eff}$ with the external field strength for the two CMG films are shown in Fig. 4. A phenomenological fitting using single exponential decay is applied to describe the field dependence as $\alpha_{\rm eff} = \alpha_0 + \alpha_{\rm ext}\ \exp(-\beta H)$,[36,37,39] where the first and second term denote the intrinsic and extrinsic damping constant, respectively, and the latter is dependent on H. The fitting results show that $\alpha_0 = 0.0055 \pm 0.0004$ for CMG1 and $\alpha_0 = 0.015 \pm 0.002$ for CMG2, indicating that the latter is about three times larger than that of the former. Moreover, compared with the previous studies,[28–30] the α_0 values for both of the present Mn-deficient CMG films are obviously larger. These results can be explained in the following.

First of all, according to the spin-orbital torque correlation model, α_0 is proportional to $\xi^2 D(E_F)/(\tau_E M_s)$,[40–42] where ξ, $D(E_F)$, and $1/\tau_E$ denote the spin-orbit coupling strength, DOS at the Fermi level, and electron scattering frequency, respectively. The room-temperature resistivities of CMG1 and CMG2 are measured to be $\sim 130\ \mu\Omega$·cm and $\sim 157\ \mu\Omega$·cm, respectively. They differ not too much and are both close to those values for single-crystalline Co_2MnGa films (120–180 μΩ·cm) reported previously,[7,16] indicating that the influence of τ_E on α_0 can be neglected. Considering that the atomic numbers of Mn (25), Co (27) and Ga (31) are small and close to each other, and the lattice constants for CMG1 and CMG2 are almost unchanged in comparison with stoichiometric CMG, ξ may change little and its influence on α_0 can also be neglected in the present Mn-deficient CMG films. However, since the compositions of the CMG films are off-stoichiometric, the band structure, $D(E_F)$, and M_s will be altered, which may affect the damping property accordingly. In order to verify this, first-principles calculations based on the density functional theory (DFT) were performed on three CMG compounds, i.e., $Co_{50}Mn_{25}Ga_{25}$, $Co_{56.25}Mn_{18.75}Ga_{25}$ (Co-rich), $Co_{50}Mn_{18.75}Ga_{31.25}$ (Ga-rich), which mimic the stoichiometric CMG, CMG1 and CMG2, respectively. The calculated DOS and the relevant parameters, e.g., lattice constants, atomic magnetic moments (m_{Co}, m_{Mn} and m_{Ga}), and total magnetic moment (m_{Total}) can be found in the Supplementary Material. These results unambiguously show that the lattice constants of the two nonstoichiometric samples change little and in the meantime the Co-rich sample has a slightly larger M_s while the Ga-rich sample has a significantly reduced M_s in comparison with the stoichiometric CMG, agreeing well with the experimental observations. Although the calculations are performed at 0 K, the thermal energy corresponding to room temperature is only about 26 meV, which has little influence on $D(E_F)$ because the DOSs of spin-up and spin-down subbands are almost unchanged within tens of meV near the Fermi level. In addition, there are certain differences between the calculated ratio of m(CMG1)/m(CMG2) and the experimental one, which may be due to the fact that the crystal defects, domain walls, non-zero temperature and the composition deviation are not considered in the

calculations.

Several groups[43–45] have presented that the magnetic properties can be well understood in terms of the hybridization between Co and Mn atoms, and the indirect exchange of the Mn d electrons through the sp atom (e.g., Ga). For the Co-rich sample, the Mn-deficient sites are occupied by excessive Co atoms, which enhances the hybridization between Co and Mn and thus the ferromagnetic coupling of Co–Co and Co–Mn, leading to prominent increases of m_{Co} and m_{Total}. If the Mn-deficient sites are occupied by the excessive Ga atoms, the hybridization between magnetic atoms will be weakened, leading to the decreases of m_{Co} and m_{Total}. On the other hand, the $D(E_{\mathrm{F}})$ will increase obviously if the composition of CMG is off-stoichiometric, as clearly illustrated by the calculated band structure. The ratios of $D(E_{\mathrm{F}})/m_{\mathrm{Total}}$ are calculated to be 2.070, 2.917, and 3.186 for $Co_{50}Mn_{25}Ga_{25}$, $Co_{56.25}Mn_{18.75}Ga_{25}$, and $Co_{50}Mn_{18.75}Ga_{31.25}$, respectively. Thus, the α_0 value can be estimated by $\alpha_0(Co_{50}Mn_{25}Ga_{25}) < \alpha_0(Co_{56.25}Mn_{18.75}Ga_{25}) < \alpha_0(Co_{50}Mn_{18.75}Ga_{31.25})$. Moreover, distinct PSSW modes were observed in our samples, providing additional channel for extra energy dissipation. Therefore, the α_0 value for CMG2 is larger than that of CMG1 and both of them are obviously larger than that of the stoichiometric CMG.

In summary, two single-crystalline Mn-deficient CMG alloy films, i.e., $Co_{55}Mn_{18}Ga_{27}$ (CMG1) and $Co_{50}Mn_{18}Ga_{32}$ (CMG2), were epitaxially grown on MgO (001) substrates. XRD characterizations demonstrate that the CMG1 film has a mixing phase of $L2_1$ and $B2$ while the CMG2 has an almost pure $B2$ phase, indicating that the former has larger chemical ordering than the latter. The in-plane M–H loops exhibit that CMG1 has an obvious in-plane magnetic anisotropy, which is almost absent in CMG2. The TRMOKE precession signals demonstrate a clear beating frequency effect in both the CMG films, indicating a considerable PSSW mode in addition to the uniform mode. The α_0 values for the two Mn-deficient CMG films are both larger than that of the stoichiometric CMG film reported previously, and meanwhile the α_0 value of CMG2 is about three times larger than that of CMG1. The magnetic damping properties of the Mn-deficient CMG films can be explained by the increase of $D(E_{\mathrm{F}})/M_{\mathrm{s}}$ in contrast to stoichiometric CMG, which can be verified by the first-principles calculations, and the excitation of PSSW mode as well. This work paves a new way for manipulating damping properties of magnetic Weyl semimetal by slight off-stoichiometry, which is of great importance in designing new generation spintronic devices.

Supplementary Material. See the supplementary material for detailed information of the following: FFT spectra at various external magnetic fields for CMG1 and CMG2; comparison of frequencies obtained by TRMOKE and FFT for CMG1 and CMG2; exclusion of Damon-Eshbach mode; first-principles calculations for stoichiometric CMG and two Mn-deficient CMG compounds of $Co_{56.25}Mn_{18.75}Ga_{25}$ and $Co_{50}Mn_{18.75}Ga_{31.25}$.

Acknowledgment. This work was supported by the National Key R&D Program of China (Grant Nos. 2022YFA1403602 and 2021YFB3601600), the National Natural Science Foundation of China (Grant Nos. 51971109, U22A20117, 51771053, 52001169, 11874199, 12104216, and 12241403), and the Natural Science Foundation of Jiangsu Province of China (Grant No. BK20200307).

References

[1] Belopolski I, Chang G, Cochran T A, Cheng Z J, Yang X P, Hugelmeyer C, Manna K, Yin J X, Cheng G, Multer D, Litskevich M, Shumiya N, Zhang S S, Shekhar C, Schröter N B M, Chikina A, Polley C, Thiagarajan B, Leandersson M, Adell J, Huang S M, Yao N, Strocov V N, Felser C, and Hasan M Z 2022 *Nature* **604** 647

[2] Wang J, Lau Y C, Zhou W, Seki T, Sakuraba Y, Kubota T, Ito K, and Takanashi K 2022 *Adv. Electron. Mater.* **8** 2101380

[3] Zhou W N, Yamamoto K, Miura A *et al.* 2021 *Nat. Mater.* **20** 463

[4] Chang G Q, Xu S Y, Zhou X T, Huang S M, Singh B, Wang B K, Belopolski I, Yin J X, Zhang S T, Bansil A, Lin H, and Hasan M Z 2017 *Phys. Rev. Lett.* **119** 156401

[5] Manna K, Sun Y, Muechler L, Kübler J, and Felser C 2018 *Nat. Rev. Mater.* **3** 244

[6] Belopolski I, Manna K, Sanchez D S, Chang G, Ernst B, Yin J, Zhang S S, Cochran T, Shumiya N, Zheng H, Singh B, Bian G, Multer D, Litskevich M, Zhou X, Huang S M, Wang B, Chang T R, Xu S Y, Bansil A, Felser C, Lin H, and Hasan M Z 2019 *Science* **365** 1278

[7] Sakai A, Mizuta Y P, Nugroho A A, Sihombing R, Koretsune T, Suzuki M T, Takemori N, Ishii R, Nishio-Hamane D, Arita R, Goswami P, and Nakatsuji S 2018 *Nat. Phys.* **14** 1119

[8] Markou A, Kriegner D, Gayles J, Zhang L, Chen Y C, Ernst B, Lai Y H, Schnelle W, Chu Y H, Sun Y, and Felser C 2019 *Phys. Rev. B* **100** 054422

[9] Reichlova H, Schlitz R, Beckert S, Swekis P, Markou A, Chen Y C, Kriegner D, Fabretti S, Park G H, Niemann A, Sudheendra S, Thomas A, Nielsch K, Felser C, and Goennenwein S T B 2018 *Appl. Phys. Lett.* **113** 212405

[10] Higo T, Man H, Gopman D B, Wu L, Koretsune T, van 't ERVE O M J, Kabanov Y P, Rees D, Li Y, Suzuki M T, Patankar S, Ikhlas M, Chien C L, Arita R, Shull R D, Orenstein J, and Nakatsuji S 2018 *Nat. Photon.* **12** 73

[11] Son D T and Spivak B Z 2013 *Phys. Rev. B* **88** 104412

[12] Zhang C L, Xu S Y, Belopolski I, Yuan Z, Lin Z, Tong B, Bian G, Alidoust N, Lee C C, Huang S M, Chang T R, Chang G, Hsu C H, Jeng H T, Neupane M, Sanchez D S, Zheng H, Wang J, Lin H, Zhang C, Lu H Z, Shen S Q, Neupert T, Hasan M Z, and Jia S 2016 *Nat. Commun.* **7** 10735

[13] Chico J, Keshavarz S, Kvashnin Y, Pereiro M, Marco I D, Etz C, Eriksson O, Bergman A, and Bergqvist L 2016 *Phys. Rev. B* **93** 214439

[14] Guillemard C, Petit-Watelot S, Devolder T, Pasquier L, Boulet P, Migot S, Ghanbaja J, Bertran F, and Andrieu S 2020 *J. Appl. Phys.* **128** 241102

[15] Varaprasad B S D C S, Rajanikanth A, Takahashi Y K, and Hono K 2010 *Appl. Phys. Express* **3** 023002

[16] Wang Q, Wen Z, Kubota T, Seki T, and Takanashi K 2019 *Appl. Phys. Lett.* **115** 252401

[17] Hellman F, Hoffman A, Tserkovnyak Y, Beach G S D, Fullerton E E, Leighton C, MacDonald A H, Ralph D C, Arena D A, Dürr H A, Fischer P, Grollier J, Heremans J P, Jungwirth T, Kimel A V, Koopmans B, Krivorotov I N, May S J, Petford-Long A K, Rondinelli J M, Samarth N, Schuller I K, Slavin A N, Stiles M D, Tchernyshyov

O, Thiavllew A, and Zink B L 2017 *Rev. Mod. Phys.* **89** 025006
[18] Tang K, Wen Z, Lau Y C, Sukegawa H, Seki T, and Mitani S 2021 *Appl. Phys. Lett.* **118** 062402
[19] Han J H, McGoldrick B C, Chou C T, Safi T S, Hou J T, and Liu L Q 2021 *Appl. Phys. Lett.* **119** 212409
[20] Žutić I, Fabian J, and Sarma S D 2004 *Rev. Mod. Phys.* **76** 323
[21] Hals K M D, Flensberg K, and Rudner M S 2015 *Phys. Rev. B* **92** 094403
[22] Ma T Y, Luo Z, Li Z W, Qiao L, Wang T, and Li F S 2019 *Chin. Phys. B* **28** 057505
[23] Benakli M, Torabi A F, Mallary M L, Zhou H, and Bertram H N 2001 *IEEE Trans. Magn.* **37** 1564
[24] Li X, Zhang Z, Jin Q Y, and Liu Y 2009 *New J. Phys.* **11** 023027
[25] Costa J D, Serrano-Guisan S, Lacoste B, Jenkins A S, Böhnert T, Tarequzzaman M, Borme J, Deepak F L, Paz E, Ventura J, Ferreira R, and Freitas P P 2017 *Sci. Rep.* **7** 7237
[26] Zhu Z, Higo T, Nakatsuji S, and Otani Y 2020 *AIP Adv.* **10** 085020
[27] Guin S N, Manna K, Noky J, Watzman S J, Fu C, Kumar N, Schnelle W, Shekhar C, Sun Y, Gooth J, and Fesler C 2019 *NPG Asia Mater.* **11** 16
[28] Guillemard C, Petit-Watelot S, Pasquier L, Pierre D, Ghanbaja J, Rojas-Sánchez J C, Bataille A, Rault J, Fèvre P L, Bertran F, and Andrieu S 2019 *Phys. Rev. Appl.* **11** 064009
[29] Guillemard C, Petit-Watelot S, Rojas-Sánchez J C, Hohlfeld J, Ghanbaja J, Bataille A, Fèvre P L, Bertran F, and Andrieu S 2019 *Appl. Phys. Lett.* **115** 172401
[30] Swekis P, Sukhanov A S, Chen Y C, Gloskovskii A, Fecher G H, Panagiotopoulos I, Sichelschmidt J, Ukleev V, Devishvili A, Vorobiev A, Inosov D S, Goennenwein S T B, Felser C, and Markou A 2021 *Nanomaterials* **11** 251
[31] Faregh R A, Boochani A, Masharian S R, and Jafarpour F H 2019 *Int. Nano Lett.* **9** 339
[32] Galanakis I and Dederichs P H 2002 *Phys. Rev. B* **66** 174429
[33] Shelke V, Srinivasan G, and Gupta A 2010 *Phys. Status Solidi (RRL)* **4** 79
[34] Tu H, Liu B, Huang D, Ruan X, You B, Huang Z, Zhai Y, Gao Y, Wang J, Wei L, Yuan Y, Xu Y, and Du J 2017 *Sci. Rep.* **7** 43971
[35] Tu H Q, Wang J, Huang Z C, Zhai Y, Zhu Z D, Hang Z, Qu J T, Zheng R K, Yuan Y, Liu R B, Zhang W, You B, and Du J 2020 *J. Phys.: Condens. Matter* **32** 335804
[36] Lu X Y, Atkinson L J, Kuerbanjiang B, Liu B, Li G Q, Wang Y, Wang J L, Ruan X Z, Wu J, Evans R F L, Lazarov V K, Chantrell R W, and Xu Y B 2019 *Appl. Phys. Lett.* **114** 192406
[37] Walowski J, Kaufmann M D, Lenk B, Hamann C, McCord J, and ünzenberg M M 2008 *J. Phys. D.* **41** 164016
[38] Lenk B, Eilers G, Hamrle J, and Münzenberg M 2010 *Phys. Rev. B* **82** 134443
[39] Liu B, Ruan X, Wu Z, Tu H, Du J, Wu J, Lu X, He L, Zhang R, and Xu Y 2016 *Appl. Phys. Lett.* **109** 042401
[40] Kamberský V 1976 *Czech. J. Phys. B* **26** 1366
[41] Kamberský V 1970 *Can. J. Phys.* **48** 2906
[42] Mizukami S, Wu F, Sakuma A, Walowski J, Watanabe D, Kubota T, Zhang X, Naganuma H, Oogane M, Ando Y, and Miyazaki T 2011 *Phys. Rev. Lett.* **106** 117201
[43] Kübler J, Williams A R, and Sommers C B 1983 *Phys. Rev. B* **28** 1745
[44] Galanakis I, Dederichs P H, and Papanikola OU N 2002 *Phys. Rev. B* **66** 134428
[45] Reitz J R and Stearns M B 1979 *J. Appl. Phys.* **50** 2066